Quantitative Approximation of the Cortical Surface Potential From EEG and ECoG Measurements

Mark A. Kramer and Andrew J. Szeri*

***Abstract*—A quantitative approximation of the cortical surface potential from measured scalp surface potential data is developed. The derivation is based on a local Taylor series expansion (TSE) in the surface normal coordinate. Analytical and numerical results for the four shell spherical head model show that the TSE method improves the spatial deblurring of the surface Laplacian method. The inclusion of the biharmonic term, the extension to other geometries, and the application to electrocorticogram measurements are discussed.**

***Index Terms*—Cortical imaging, high-resolution ECoG, high-resolution EEG, spatial deblurring, surface Laplacian.**

I. Introduction

THE electroencephalogram (EEG) provides neuroscientists with temporal and spatial maps of the scalp surface potential. Although unsurpassed in temporal resolution, the scalp EEG suffers from limited spatial resolution due to large variations in conductivity between the cerebrospinal fluid (CSF), the skull, and the scalp. Over the past few decades, neuroscientists have found methods to improve the limited spatial resolution of scalp EEG and to approximate the cortical surface potential. These high-resolution EEG techniques are valuable both intrinsically and as a processing step to precede other analysis, such as source localization. Techniques developed to improve the spatial resolution of scalp EEG can be divided into two categories: harmonic continuation techniques [1], [2] and surface Laplacian techniques [3], [4].

In [2], a technique of harmonic continuation is described. The scalp surface potential is fitted with an expansion in terms of Legendre functions. Because there are no current sources within the scalp, the scalp potential satisfies Laplace's equation. Hence, the way in which the coefficients of the terms in the Legendre function expansion vary with radial coordinate is determined by their order. With this knowledge, the scalp potential may be evaluated on the skull surface. The continuity of the potential and of the radial component of the current density permit further continuation into the skull, and so on. In this way, the harmonic nature of the potential in the scalp, skull, and CSF may be exploited to render the potential on the cortical surface. Among the drawbacks to this technique are that it relies on the analytic determination of the scalp surface potential in terms of Legendre functions and that the projection coefficients that facilitate the downward continuation are difficult to evaluate analytically for more realistic geometries.

Another technique to improve the spatial resolution of scalp EEG involves the application of the surface Laplacian (SL). The SL is a mathematical operator one can apply to a function over any smooth, two-dimensional (2-D) surface. By associating this mathematical operator with a field theory of electromagnetism appropriate to neural activity, one can develop meaningful physical quantities, such as the scalp current density (SCD) [5]. The SL of the scalp potential also provides a noninvasive, qualitative estimation of the cortical surface potential [4]. In Section II of this paper, we review this application of the SL.

The plan for the remainder of this paper is as follows. In Section III, we present a new method for determining a quantitative approximation to the cortical surface potential based on a Taylor series expansion (TSE) in the surface normal coordinate. We examine the TSE method analytically and through computer simulations, as well as discuss spatial sampling and electrocorticogram (ECoG) measurements, in Section IV. Finally, in Section V, we summarize the results.

II. SL Cortical Surface Potential Estimation

The combination of the high-conductivity CSF and low-conductivity skull spreads current from a cortical source over a wide region of scalp. This spatial spreading of current blurs the potential distributions of nearby cortical sources, rendering them less distinguishable in scalp EEG. The goal of cortical imaging is to undo this blurring and thereby to approximate the cortical surface potential. After an insightful physical argument and numerous computer simulations, Nunez *et al.* [4] show that the SL $\nabla_{||}^2$ of the scalp surface potential Φ_0 can be used to estimate the cortical surface potential Φ_x through the proportional relation

$$\Phi_x \propto \Phi_0 - A_{KS}\nabla_{||}^2\Phi_0 \tag{1}$$

where A_{KS} is the numerical factor

$$A_{KS} \approx r_k r_c \frac{\sigma_c}{\sigma_k}. \tag{2}$$

Here, r_k and r_c are the thicknesses of the skull and scalp, and σ_k and σ_c are the skull and scalp conductivities, respectively. Thus, knowing the scalp potential Φ_0 and the values of the physical quantities in (2), the cortical surface potential Φ_x is approximated by (1). In practice, the cortical potential is visualized more simply as

$$\Phi_x \propto -\nabla_{||}^2\Phi_0 \tag{3}$$

Manuscript received June 3, 2003; revised October 19, 2003. The work of M. A. Kramer was supported in part by the National Science Foundation (NSF) under a Graduate Research Fellowship. *Asterisk indicates corresponding author.*

M. A. Kramer is with the Graduate Group in Applied Science and Technology, University of California, Berkeley, CA 94720-1708 USA (e-mail: markram@berkeley.edu).

*A. J. Szeri is with the the Graduate Group in Applied Science and Technology and the Department of Mechanical Engineering, University of California, Berkeley, CA 94720-1740 USA (e-mail: aszeri@me.berkeley.edu).

Digital Object Identifier 10.1109/TBME.2004.827264

TABLE I
FOUR-SHELL SPHERICAL HEAD MODEL PARAMETERS

Layer	Potential	Inner Radius (cm)	Conductivity (S/m)
Air	Φ_a	δ (9.2) $\leq$ r $\leq \infty$	σ_a (0.0)
Scalp	Φ_c	γ (8.7) $\leq$ r $\leq \delta$	σ_c (0.44)
Skull	Φ_k	β (8.2) $\leq$ r $\leq \gamma$	σ_k (0.015)
CSF	Φ_f	α (8.0) $\leq$ r $\leq \beta$	σ_f (1.8)
Brain	Φ_b	0 $\leq$ r $\leq \alpha$	σ_b (0.15)

The numerical values are from [7].

because the magnitude of the second term in (1) greatly exceeds that of the first, as verified experimentally [4]. Although derived for a spherical head model, (3) may be applied to more realistic geometries [3], [6]. The main advantages of using (3) to approximate Φ_x are its model independence and simple implementation.

The justification of (1) is based on physical approximations and computer simulations [3], [4]. In what follows, we present a method of approximating the cortical surface potential based on a TSE in the surface normal coordinate. We find that the largest terms in the expression match those of (1). However, there are higher order terms whose neglect gives information about errors in the use of (1). Moreover, the new expression we develop to replace (1) is quantitative and not simply proportional to Φ_x.

III. TSE METHOD

The TSE of the scalp surface potential provides an approximation to the cortical surface potential. For simplicity and concreteness, the formulation is derived here for a four-shell spherical head model with parameters listed in Table I. The extension of this derivation to other geometries is discussed in Appendix II. The computation involves two steps: 1) determination of the TSE in r of the potential in each layer of the model and 2) exploitation of the boundary conditions at each interface of the model. The application of this process to each layer of the four shell spherical head model is discussed in what follows.

The first step in the TSE procedure is to approximate the potential $\Phi_c[\gamma \leq r \leq \delta, \theta, \phi]$ within the scalp given the scalp surface potential $\Phi_c[\delta, \theta, \phi] \equiv \Phi_0[\theta, \phi]$ at the air/scalp interface $r = \delta$. In general, we can expand any well-behaved function of (r, θ, ϕ) near $r = r_0$ in a Taylor series

$$\Phi[r,\theta,\phi] = \Phi[r_0,\theta,\phi] + (r-r_0)\partial_r\Phi[r,\theta,\phi]|_{r_0} + \frac{1}{2}(r-r_0)^2\partial_r^2\Phi[r,\theta,\phi]|_{r_0} + O[(r-r_0)^3]. \quad (4)$$

Here, $O[(r-r_0)^3]$ includes all terms of order $(r-r_0)^3$ and higher and $\partial_r^n\Phi|_{r_0} \equiv (\partial^n\Phi/\partial r^n)|_{r=r_0}$. To determine the potential within the scalp $\Phi_c[r,\theta,\phi]$ from the scalp surface potential $\Phi_0[\theta,\phi]$, we fix $r_0 = \delta$ in (4) and write

$$\Phi_c[r,\theta,\phi] = \Phi_c[\delta,\theta,\phi] + (r-\delta)\partial_r\Phi_c[r,\theta,\phi]|_\delta + \frac{1}{2}(r-\delta)^2\partial_r^2\Phi_c[r,\theta,\phi]|_\delta + O[(r-\delta)^3]. \quad (5)$$

Because the unknown function $\Phi_c[r,\theta,\phi]$ occurs on both sides of (5), we express the right-hand side of this equation in terms of the known scalp surface potential $\Phi_0[\theta,\phi]$. To do so requires exploitation of the boundary conditions at the air/scalp interface. In general, at the interface r_{ij} of shells i and j we have

$$\Phi_i[r_{ij},\theta,\phi] = \Phi_j[r_{ij},\theta,\phi] \quad (6)$$

$$\sigma_i\partial_r\Phi_i[r,\theta,\phi]|_{r_{ij}} = \sigma_j\partial_r\Phi_j[r,\theta,\phi]|_{r_{ij}} \quad (7)$$

where σ_i and σ_j are the conductivities of layers i and j, respectively [8]. Then, the first term of (5) is simply related to the scalp surface potential

$$\Phi_c[\delta,\theta,\phi] = \Phi_0[\theta,\phi] \quad (8)$$

by use of (6). For the second term of (5), we must determine the normal derivative of $\Phi_c[r,\theta,\phi]$ evaluated at the air/scalp interface $r = \delta$. Equation (7) yields

$$\partial_r\Phi_c[r,\theta,\phi]|_\delta = \frac{\sigma_a}{\sigma_c}\partial_r\Phi_a[r,\theta,\phi]|_\delta \quad (9)$$

where $\Phi_a[r,\theta,\phi]$ is the potential of the air surrounding the scalp and σ_a and σ_c are the conductivities of the air and scalp, respectively. Because $\sigma_a \approx 0$, we conclude

$$\partial_r\Phi_c[r,\theta,\phi]|_\delta = 0. \quad (10)$$

Finally, for the third term in (5), recall that all current sources are located in the cortex. Then Laplace's equation $\nabla^2\Phi_c[r,\theta,\phi] = 0$ holds in the scalp. We write the Laplacian in spherical coordinates and solve for $\partial_r^2\Phi_c[r,\theta,\phi]$ to obtain

$$\begin{aligned}\partial_r^2\Phi_c[r,\theta,\phi]|_\delta &= -\frac{2}{\delta}\partial_r\Phi_c[r,\theta,\phi]|_\delta - \frac{1}{\delta^2}\nabla_{||}^2\Phi_c[r,\theta,\phi]|_\delta \\ &= -\frac{2}{\delta}\frac{\sigma_a}{\sigma_c}\partial_r\Phi_a[r,\theta,\phi]|_\delta - \frac{1}{\delta^2}\nabla_{||}^2\Phi_c[r,\theta,\phi]|_\delta \\ &= -\frac{1}{\delta^2}\nabla_{||}^2\Phi_0[\theta,\phi]. \end{aligned} \quad (11)$$

Here, we have made use of (8), (9), and $\sigma_a \approx 0$. We remark that, for simplicity, we are defining

$$\nabla_{||}^2[\cdot] \equiv \frac{1}{\sin\theta}\partial_\theta(\sin\theta\,\partial_\theta[\cdot]) + \frac{1}{\sin^2\theta}\partial_\phi^2[\cdot] \quad (12)$$

rather than

$$\nabla_{||}^2[\cdot] \equiv \frac{1}{r^2\sin\theta}\partial_\theta(\sin\theta\partial_\theta[\cdot]) + \frac{1}{r^2\sin^2\theta}\partial_\phi^2[\cdot]. \quad (13)$$

This will save having to define different SL operators at different radii and hence simplify the notation. We combine the results for all three terms in (5) to conclude

$$\Phi_c[r,\theta,\phi] = \Phi_0[\theta,\phi] - \frac{(r-\delta)^2}{2\delta^2}\nabla_{||}^2\Phi_0[\theta,\phi] + O[(r-\delta)^3]. \quad (14)$$

Hence, we have expressed the potential distribution within the scalp $\Phi_c[\gamma \leq r \leq \delta, \theta, \phi]$ in terms of the potential distribution at the air/scalp interface $\Phi_0[\theta,\phi]$ using only the approximations of a TSE and of $\sigma_a \approx 0$. We regroup the terms in (14) and express the scalp potential as an operator acting on $\Phi_0[\theta,\phi]$

$$\Phi_c[r,\theta,\phi] = \left(1 - \frac{(r-\delta)^2}{2\delta^2}\nabla_{||}^2\right)\Phi_0[\theta,\phi] + O[(r-\delta)^3]. \quad (15)$$

Equation (15) is the approximation to the potential at any radius r within the scalp $(\gamma \leq r \leq \delta)$ given the potential recorded at the air/scalp interface $\Phi_0[\theta,\phi]$, and the error is $O[(r-\delta)^3]$. With the goal of approximating the cortical surface potential, we continue the estimation process through the next layer of the model: the skull.

To find the potential distribution within the skull $\Phi_k[\beta \leq r \leq \gamma, \theta, \phi]$, we follow the same procedures as above. When

$r = \gamma$, (15) is the approximation of the potential distribution at the scalp/skull interface. We calculate from (4) the TSE of the potential within the skull

$$\Phi_k[r,\theta,\phi] = \Phi_k[\gamma,\theta,\phi] + (r-\gamma)\partial_r\Phi_k[r,\theta,\phi]|_\gamma + \frac{1}{2}(r-\gamma)^2\partial_r^2\Phi_k[r,\theta,\phi]|_\gamma + O[(r-\gamma)^3]. \quad (16)$$

We express the right-hand side in terms of $\Phi_c[r,\theta,\phi]$ for which we have developed the approximation (15). Then, the first term in (16) is

$$\Phi_k[\gamma,\theta,\phi] = \Phi_c[\gamma,\theta,\phi] = \left(1 - \frac{(\gamma-\delta)^2}{2\delta^2}\nabla_{\|}^2\right)\Phi_0[\theta,\phi] + O[(\gamma-\delta)^3] \quad (17)$$

by continuity (6), (9), and (15). The second expansion term in (16) is, by use of (7) and (15),

$$\partial_r\Phi_k[r,\theta,\phi]|_\gamma = -\frac{\sigma_c}{\sigma_k}\frac{(\gamma-\delta)}{\delta^2}\nabla_{\|}^2\Phi_0[\theta,\phi] + O[(\gamma-\delta)^2]. \quad (18)$$

The third term of (16) can be written as

$$\partial_r^2\Phi_k[r,\theta,\phi]|_\gamma = -\frac{2}{\gamma}\partial_r\Phi_k[r,\theta,\phi]|_\gamma - \frac{1}{\gamma^2}\nabla_{\|}^2\Phi_k[r,\theta,\phi]|_\gamma \quad (19)$$

and evaluated using (7), (15), and (18). Here, we have made use of the fact that there are no sources in $\beta \le r \le \gamma$. We substitute these results into (16) and simplify to obtain the approximate skull potential distribution

$$\begin{aligned}\Phi_k[r,\theta,\phi] = \Bigg\{1 &+ \left(-\frac{(\gamma-\delta)^2}{2\delta^2} - \frac{(r-\gamma)(\gamma-\delta)}{\delta^2}\frac{\sigma_c}{\sigma_k} + \frac{(r-\gamma)^2(\gamma-\delta)}{\gamma\delta^2}\frac{\sigma_c}{\sigma_k} - \frac{(r-\gamma)^2}{2\gamma^2}\right)\nabla_{\|}^2 \\ &+ \left(\frac{(r-\gamma)^2(\gamma-\delta)^2}{4\gamma^2\delta^2}\right)\nabla_{\|}^4\Bigg\}\Phi_0[\theta,\phi] \\ &+ O[(\gamma-\delta)^3] + O[(r-\gamma)(\gamma-\delta)^2] \\ &+ O[(r-\gamma)^2(\gamma-\delta)] + O[(r-\gamma)^3] \quad (20)\end{aligned}$$

where $\beta \le r \le \gamma$ and $\nabla_{\|}^4$ is the surface biharmonic operator, which, like (12), is dimensionless. This expression may be used to approximate the potential distribution at the skull/CSF interface, $\Phi_k[r = \beta,\theta,\phi]$. Finally, we follow the same procedures as before and approximate the potential distribution within the CSF, $\Phi_f[\alpha \le r \le \beta,\theta,\phi]$. Evaluation of $\Phi_f[r = \alpha,\theta,\phi]$ at the CSF/cortex interface produces the final result, an approximation of the cortical surface potential $\Phi_x[\theta,\phi]$ from the recorded scalp surface potential $\Phi_0[\theta,\phi]$. We find

$$\begin{aligned}\Phi_x[\theta,\phi] \approx \Bigg\{1 &+ \Bigg[\left(-\frac{(\alpha-\beta)^2}{2\beta^2} - \frac{(\beta-\gamma)^2}{2\gamma^2} - \frac{(\gamma-\delta)^2}{2\delta^2}\right) \\ &+ \left(\frac{(\beta-\alpha)(\gamma-\delta)}{\delta^2} + \frac{(\alpha-\beta)^2(\gamma-\delta)}{\beta\delta^2}\right)\frac{\sigma_c}{\sigma_f} \\ &+ \left(\frac{(\beta-\alpha)(\beta-\gamma)}{\gamma^2} + \frac{(\alpha-\beta)^2(\beta-\gamma)}{\beta\gamma^2}\right)\frac{\sigma_k}{\sigma_f} \\ &+ \left(\frac{(\beta-\gamma)^2(\gamma-\delta)}{\gamma\delta^2} + \frac{(\gamma-\beta)(\gamma-\delta)}{\delta^2}\right)\frac{\sigma_c}{\sigma_k} \\ &- 2\left(\frac{(\alpha-\beta)(\beta-\gamma)(\gamma-\delta)}{\gamma\delta^2}\right. \\ &\left. + \frac{(\alpha-\beta)^2(\beta-\gamma)(\gamma-\delta)}{\beta\gamma\delta^2}\right)\frac{\sigma_c}{\sigma_f}\Bigg]\nabla_{\|}^2 \\ &+ \Bigg[\left(\frac{(\alpha-\beta)^2(\beta-\gamma)^2}{4\beta^2\gamma^2} + \frac{(\alpha-\beta)^2(\gamma-\delta)^2}{4\beta^2\delta^2} + \frac{(\beta-\gamma)^2(\gamma-\delta)^2}{4\gamma^2\delta^2}\right) \\ &+ \left(\frac{(\alpha-\beta)^2(\beta-\gamma)(\gamma-\delta)}{2\beta^2\delta^2} + \frac{(\alpha-\beta)^2(\beta-\gamma)^2(\delta-\gamma)}{2\beta^2\gamma\delta^2}\right)\frac{\sigma_c}{\sigma_k} \\ &+ \left(\frac{(\beta-\alpha)(\gamma-\beta)(\gamma-\delta)^2}{2\gamma^2\delta^2} + \frac{(\alpha-\beta)^2(\gamma-\beta)(\gamma-\delta)^2}{2\beta\gamma^2\delta^2}\right)\frac{\sigma_k}{\sigma_f}\Bigg]\nabla_{\|}^4 \\ &- \left[\frac{(\alpha-\beta)^2(\beta-\gamma)^2(\gamma-\delta)^2}{8\beta^2\gamma^2\delta^2}\right]\nabla_{\|}^6\Bigg\}\Phi_0[\theta,\phi] \quad (21)\end{aligned}$$

with error

$$\begin{aligned}&O[(\gamma-\delta)^3] + O[(\beta-\gamma)(\gamma-\delta)^2] + O[(\beta-\gamma)^2(\gamma-\delta)] \\ &\quad + O[(\beta-\gamma)^3] + O[(\alpha-\beta)(\gamma-\delta)^2] \\ &\quad + O[(\alpha-\beta)(\beta-\gamma)(\gamma-\delta)] + O[(\alpha-\beta)(\beta-\gamma)^2] \\ &\quad + O[(\alpha-\beta)^2(\gamma-\delta)] + O[(\alpha-\beta)^2(\beta-\gamma)]. \quad (22)\end{aligned}$$

We substitute in numerical values for the conductivities and radii from Table I and find

$$\Phi_x[\theta,\phi] = (1 - 0.095\,388\nabla_{\|}^2 + 3.0638\times10^{-5}\nabla_{\|}^4 - 7.254\,51\times10^{-10}\,\nabla_{\|}^6)\Phi_0[\theta,\phi] + \ldots \quad (23)$$

as the approximation to the cortical surface potential. Note that the operators in (23) are dimensionless.

A. Comparison to Prior Theory

We remark that the first two terms of (23) (i.e., the constant 1 and $\nabla_{\|}^2$) are in the same form as the expression developed in [4] and restated in (1). Examination of the coefficient of $\nabla_{\|}^2$ in (21) reveals a single dominant term

$$-\frac{(\gamma-\beta)(\delta-\gamma)}{\delta^2}\frac{\sigma_c}{\sigma_k} \quad (24)$$

due to the large value of the conductivity ratio $\sigma_c/\sigma_k \approx 30$. This matches (1) because $\nabla_{\|}^2$ in (1) includes a factor of $1/\delta^2$. We note that, in place of the factor 0.095 388 in (23) obtained by use of all the terms in (21), one finds instead 0.08664 when using only the dominant term (24). This represents an error of approximately 10%. It is interesting that the two different methods—the physical arguments of [4] and the TSE above—produce approximately the same result.

The value of having developed (21) by a different means is as follows. First, we have an idea of the errors involved in simply keeping a few of the many terms of (21) or (23). Second, the new approximation for the cortical surface potential is quantitative, rather than the proportional statement (1). Third, there may be situations where the higher order terms are of importance. Fourth, the TSE method is a local approximation and, therefore, permits changes in the model parameters—radii and conductivities, in this case—within local angular regions. There

is no built-in assumption or requirement of global consistency in the TSE method. In what follows, we discuss first-order [up to $\nabla_{\|}^2$ in (23)] and second-order [up to $\nabla_{\|}^4$ in (23)] corrections to the cortical surface potential approximation.

IV. Results

A. Analytical Consideration of TSE

For the four-shell spherical head model, there exists an analytic solution for the potential distribution due to a point current source. By superposition, more general sources—such as dipoles—may be constructed. The potential distributions due to a point current source are written compactly in terms of the spherical harmonics $Y_L^M[\theta,\phi]$ as follows:

$$\Phi_i[r,\theta,\phi]=\sum_{L=0}^{\infty}\sum_{M=-L}^{L}\left(A_i[L,M]r^L+\frac{B_i[L,M]}{r^{(L+1)}}\right)Y_L^M[\theta,\phi] \tag{25}$$

where (θ,ϕ) is the angular location of the observation point, $i=\{c,k,f,b\}$ for the scalp, skull, CSF, and brain, respectively, and the coefficients $A_i[L,M]$ and $B_i[L,M]$ are determined by matching the boundary conditions at the shell interfaces [9]. The spherical harmonics $Y_L^M[\theta,\phi]$ are defined as

$$Y_L^M[\theta,\phi]=\sqrt{\frac{2L+1}{4\pi}}\sqrt{\frac{(L-M)!}{(L+M)!}}P_L^M[\cos\theta]e^{\imath M\phi} \tag{26}$$

where $P_L^M[x]$ are the associated Legendre polynomials and $\imath=\sqrt{-1}$. For the four-shell spherical head model, an expression can be derived for the coefficients $A_i[L,M]$ and $B_i[L,M]$ within each layer i. If we divide the coefficients at the scalp surface $r=\delta$ ($B_c[L,M]$ and $A_c[L,M]$, where $A_c[L,M]=0$) by the coefficients at the cortical surface $r=\alpha$ ($A_f[L,M]$ and $B_f[L,M]$), we determine the transfer function $\mathrm{TF}[L]$ of the potential as a function of L as follows:

$$\mathrm{TF}[L]=\frac{B_c[L,M]\delta^{-(L+1)}}{A_f[L,M]\alpha^L+B_f[L,M]\alpha^{-(L+1)}}. \tag{27}$$

We note that $\mathrm{TF}[L]$ is independent of M. This is the case because the boundary conditions (6) and (7) only involve derivatives with respect to r, which makes the L dependence of $A_i[L,M]$ and $B_i[L,M]$ complicated. The coefficients $A_i[L,M]$ and $B_i[L,M]$ depend on M only through the source term, and in the ratio (27) parameters related to the source vanish.

Given a spherical harmonic of order L,M on the cortical surface, the scalp transfer function (27) determines the contribution of this spherical harmonic on the scalp surface. In Fig. 1, we plot $\mathrm{TF}[L]$ (solid curve) using the physical parameters in Table I. Owing to the conductive properties of the brain, CSF, skull, and scalp, the transfer function rapidly approaches zero as L increases. Thus, higher order spherical harmonics present on the cortical surface are strongly damped at the scalp surface.

The goal of any deblurring procedure is to eliminate the blurring produced by anisotropic and low-conductivity media by amplifying higher order spherical harmonic terms damped at the scalp surface. An ideal deblurring algorithm would be the inverse transfer function (ITF). Given the scalp surface potential, the ITF determines the undamped contribution of each spherical harmonic on the cortical surface. We note that, for this simple example, the exact ITF is the reciprocal of (27).

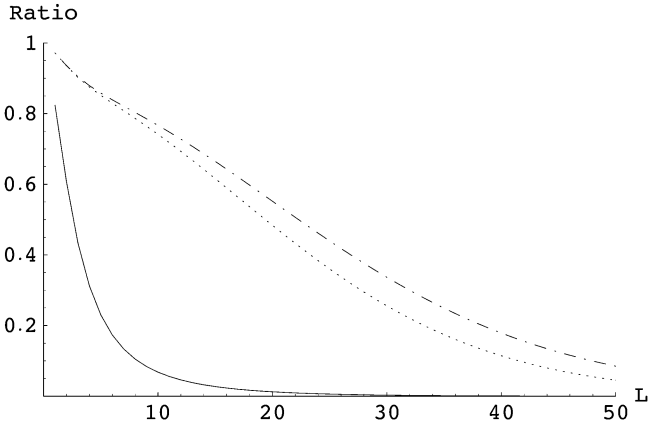

Fig. 1. Scalp transfer function $\mathrm{TF}[L]$ (solid) of a spherical harmonic term of unit magnitude on the cortical surface to the scalp surface. Higher order spherical harmonic terms are damped. Also plotted are the products of $\mathrm{TF}[L]$ with the inverse transfer functions from the scalp surface to the cortical surface ($\mathrm{ITF}_1[L]$ and $\mathrm{ITF}_2[L]$). We show the product of the scalp transfer function and the inverse transfer function for the TSE method up to the Laplacian correction ($\mathrm{TF}\times\mathrm{ITF}_1[L]$) (dotted), and the product of the scalp transfer function and the inverse transfer function for the TSE method up to the biharmonic correction ($\mathrm{TF}\times\mathrm{ITF}_2[L]$) (dot–dash line).

The TSE method determines an approximation to the ITF $\mathrm{ITF}[L]$. To see this, note that the scalp surface potential can be written as

$$\Phi_0[\theta,\phi]=\sum_{L=0}^{\infty}\sum_{M=-L}^{L}a[L,M]Y_L^M[\theta,\phi] \tag{28}$$

where the $a[L,M]$ are unknown coefficients dependent on the model parameters (i.e., the radii and conductivities of the shells, in this case). Similarly,

$$\Phi_x[\theta,\phi]=\sum_{L=0}^{\infty}\sum_{M=-L}^{L}b[L,M]Y_L^M[\theta,\phi] \tag{29}$$

for the cortical surface potential. We apply the TSE method (23) to (28) and determine an approximation of the cortical surface potential to yield

$$\Phi_x[\theta,\phi]\approx\sum_{L=0}^{\infty}\sum_{M=-L}^{L}\left(1+0.095L(L+1)+\frac{L^2(L+1)^2}{3.3\times10^4}\right)a[L,M]Y_L^M[\theta,\phi] \tag{30}$$

where we have used the well-known identity

$$\nabla_{\|}^2Y_L^M[\theta,\phi]=-L(L+1)Y_L^M[\theta,\phi]. \tag{31}$$

Then, from (29) and (30), we have

$$\begin{aligned}b[L,M]&\approx\bar{b}_1[L,M]=(1+0.095L(L+1))a[L,M]\\&\approx\bar{b}_2[L,M]=\left(1+0.095L(L+1)+\frac{L^2(L+1)^2}{3.3\times10^4}\right)a[L,M]\end{aligned} \tag{32}$$

where $\bar{b}_1[L,M]$ and $\bar{b}_2[L,M]$ correspond to first-order (up through $\nabla_{\|}^2$) and second-order (up through $\nabla_{\|}^4$) approximations to $b[L,M]$, respectively. The factors preceding $a[L,M]$ in (32) approximate the ITFs; given $a[L,M]$, corresponding to

the scalp surface potential, the first- and second-order ITFs, defined as

$$\begin{aligned}\mathrm{ITF}_1[L] &= 1 + 0.095L(L+1) \\ \mathrm{ITF}_2[L] &= 1 + 0.095L(L+1) + \frac{L^2(L+1)^2}{3.3 \times 10^4}\end{aligned} \tag{33}$$

determine an approximation to $b[L, M]$. To analyze the approximations (32), we plot the ratios of the approximate cortical coefficients in (32) to the exact cortical coefficient

$$\begin{aligned}\frac{\overline{b}_1[L,M]}{b[L,M]} &= (1 + 0.095L(L+1))\frac{a[L,M]}{b[L,M]} \\ &= \mathrm{ITF}_1[L] \times \mathrm{TF}[L]\end{aligned} \tag{34}$$

and

$$\begin{aligned}\frac{\overline{b}_2[L,M]}{b[L,M]} &= \left(1 + 0.095L(L+1) + \frac{L^2(L+1)^2}{3.3 \times 10^4}\right)\frac{a[L,M]}{b[L,M]} \\ &= \mathrm{ITF}_2[L] \times \mathrm{TF}[L]\end{aligned} \tag{35}$$

in Fig. 1. Here, we have used the definitions (33) and the definition of $\mathrm{TF}[L]$. If $\mathrm{ITF}_1[L]$ or $\mathrm{ITF}_2[L]$ were the exact ITF, then the ratio (34) or (35) would equal one. We show in Fig. 1 that both ratios decrease as L increases, though much less rapidly than $\mathrm{TF}[L]$ does. The higher order L contributes more to $\mathrm{ITF}_2[L]$, due to the inclusion of the biharmonic term in (35). In Appendix I, we show that for $L \geq 17$ the contribution of the biharmonic term is important (i.e., contributes more than 10% to the TSE approximation). The TSE method increases the contribution of higher order spherical harmonic terms in the scalp potential distribution and thereby approximates the cortical surface potential.

B. Application of TSE To ECoG Measurements

The discussion has been focused thus far on deblurring the scalp surface potential. In ECoG measurements, the electric potential is recorded at layer I of the cortex, above the source distributions in layers III or IV of the cortex. These measurements, although closer to the source distribution, are still spatially blurred by the intervening material. By modifying the numerical values in Table I, we can apply the TSE method to ECoG measurements. We set all of the nonzero conductivities equal to σ_b and $(\alpha, \beta, \gamma, \delta) = (8.0, 8.03, 8.06, 8.09)$ to approximate a thin layer (0.9 mm) of material separating the ECoG measurement from the current source distribution at r =7.99 cm. With these numerical values, the replacement to (23) is

$$\begin{aligned}\Phi_x[\alpha,\theta,\phi] \approx (1 - 6.2 \times 10^{-5}\,\nabla_{||}^2 \\ + 3.4 \times 10^{-10}\,\nabla_{||}^4)\Phi_0[\delta,\theta,\phi].\end{aligned} \tag{36}$$

The transfer function and ITFs for the ECoG measurement are used to create the plots in Fig. 2. We note that the transfer function for the ECoG measurement, although broader than the scalp transfer function (27), still decreases rapidly as L increases. As in Section IV-A, we apply the ITFs from the TSE algorithm and show the increased contribution of higher order spherical harmonic terms in Fig. 2. Notice that both the first- and second-order ITFs are excellent approximations to the exact ITF up to $L = 45$.

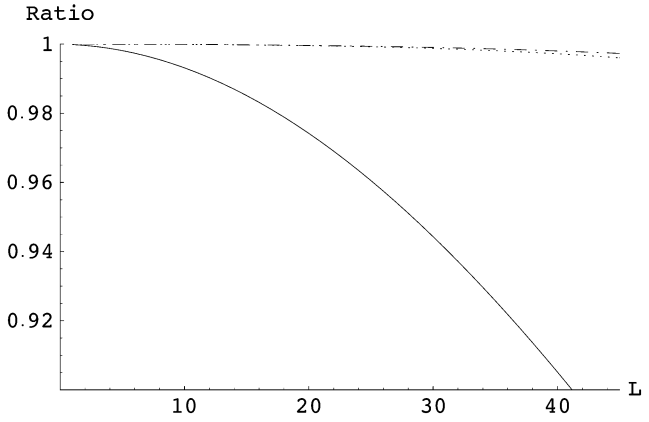

Fig. 2. ECoG transfer function $\mathrm{TF}[L]$ (solid line) of a spherical harmonic term of unit magnitude in layer IV of the cortex to layer I of the cortex. Higher order spherical harmonic terms are damped. Also plotted are the products of $\mathrm{TF}[L]$ with the ITFs from layer I of the cortex to layer IV of the cortex ($\mathrm{ITF}_1[L]$ and $\mathrm{ITF}_2[L]$). We show the product of the scalp transfer function and the ITF for the TSE method up to the Laplacian correction ($\mathrm{TF} \times \mathrm{ITF}_1[L]$) (dotted line), and the product of the scalp transfer function and the ITF for the TSE method up to the biharmonic correction ($\mathrm{TF} \times \mathrm{ITF}_2[L]$) (dot–dashed line).

C. Spatial Sampling

The results in Figs. 1 and 2 are independent of electrode spacing. By introducing an electrode configuration, the maximum observable spatial frequency becomes

$$f = \frac{1}{2\Delta\Omega} \tag{37}$$

where $\Delta\Omega$ is the angle between electrodes assumed to lie on a sphere. Given a uniform electrode spacing, we can determine the maximum order L, M of an observable spherical harmonic. The frequency f_M (in cycles per π) in the ϕ direction is

$$f_M = \frac{1}{2}M \tag{38}$$

which follows immediately from the definition of $Y_L^M[\theta, \phi]$. We define the frequency f_L (in cycles per π) in the θ direction as the frequency of maximum power in the power spectrum of Legendre polynomial L. We find that the relationship between L and f_L is approximately linear

$$f_L \approx \frac{1}{2}L. \tag{39}$$

From (37)–(39), the maximum observable order L, M as a function of electrode spacing $\Delta\Omega$ is

$$L = M \approx \frac{\pi}{\Delta\Omega}. \tag{40}$$

For example, given a uniform electrode spacing with $\Delta\Omega = (\pi/10)$, corresponding roughly to the standard 127-electrode configuration, the maximum observable spherical harmonic is of order $L = M = 10$. Our analysis of the transfer functions for this electrode configuration is then useful only up to $L = M = 10$, where the Laplacian term in (21) dominates. For an electrode spacing of $\Delta\Omega = 0.015$, possible in ECoG measurements with a high-density electrode grid, the maximum observable spherical harmonic is approximately of order $L = M = 210$. At this order, the biharmonic contribution to the TSE approximation dominates.

TABLE II
MEAN CORRELATION COEFFICIENTS

Noise	CC_0	CC_1	CC_2	CC_{SL}
None	0.73 ± 0.02	0.82 ± 0.01	0.82 ± 0.01	0.77 ± 0.02
10%	0.72 ± 0.02	0.77 ± 0.02	0.77 ± 0.02	0.73 ± 0.04

The mean CCs between the exact cortical surface potential and: the scalp surface potential (CC_0), the first order TSE (CC_1), the second order TSE (CC_2), and the traditional surface Laplacian method (CC_{SL}). The results are averaged over 100 examples of random background scalp potentials. In the first row, the noiseless scalp potential was deblurred. In the second row, 10% white noise was added to the scalp potential before deblurring.

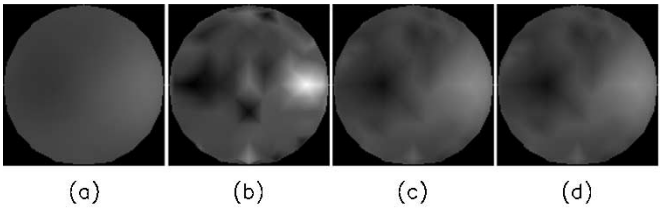

Fig. 3. Computer simulations of the potential distribution created by 220 radial dipolar current sources recorded with a standard 127-electrode configuration. (a)–(d) correspond to the (noiseless) scalp surface potential, the exact cortical surface potential, the TSE to first-order correction, and the TSE to second-order correction, respectively. The gray scales correspond in the four figures.

D. Numerical Analysis of the TSE Method

The robustness of the TSE method was tested through computer simulations. A four-shell spherical head model was chosen with the parameters listed in Table I. Two hundred and twenty dipolar radial current sources at radius r =7.99 cm (i.e., 0.1 mm below the cortical surface) were distributed uniformly in the upper hemisphere. The source currents at most sites were randomly chosen to establish a background scalp potential of ± 100 μV. In addition, source currents were assigned to create one positive $(\theta = \pi/4, \phi = \pi/2)$ and one negative $(\theta = \pi/20, \phi = 3\pi/2)$ source clump, with peak scalp potentials of ± 600 μV. Spherical harmonics up to order $L = 50$ were used to calculate the scalp and cortical surface potentials created by each source for a standard 127-scalp-electrode configuration. The TSE algorithm (23) was applied to noiseless and noisy (uniformly distributed noise bounded by ± 60 μV) scalp surface potential data and compared to the exact cortical surface potential.

To compute the surface Laplacian and biharmonic corrections in the TSE method, we utilized spline interpolation with the appropriate regularization necessary for noisy data [2], [10], [11]. The scalp surface potential $\Phi_0[\theta_i, \phi_i]$ recorded at electrode i was approximated with the surface spline functions $g_m[\cos(\omega_{ij})]$ as

$$\Phi_0[\theta_i, \phi_i] = c_0 + \sum_{j=1}^{N_e} c_j g_m[\cos(\omega_{ij})] \tag{41}$$

where $\cos(\omega_{ij})$ is the cosine of the angle between electrodes i and j, N_e is the total number of electrodes, and the c_i's are unknown coefficients. The surface spline functions are defined as

$$g_m[x] = \frac{1}{4\pi} \sum_{n=1}^{\infty} \frac{2n+1}{(n(n+1))^m} P_n[x] \tag{42}$$

where $P_n[x]$ are the Legendre polynomials of order n. For the simulations, we chose $m = 3$. After spline interpolation, the angular component of the surface Laplacian at electrode i is simply

$$\nabla^2_{||} \Phi_0[\theta_i, \phi_i] = -\sum_{j=1}^{N_e} c_j g_{m-1}[\cos(\omega_{ij})]. \tag{43}$$

Note that the argument m to the spline function decreases by 1 in (43) compared to (41). For the surface biharmonic at electrode i we have

$$\nabla^4_{||} \Phi_0[\theta_i, \phi_i] = \sum_{j=1}^{N_e} c_j g_{m-2}[\cos(\omega_{ij})] \tag{44}$$

where m has decreased by 2. We made use of the spline interpolation method and approximated the cortical surface potential with the first- (up through $\nabla^2_{||}$) and second-order (up through $\nabla^4_{||}$) corrections in (23) using (43) and (44), respectively. The linear Pearson correlation coefficients (CCs) between the exact cortical surface potential and: the scalp surface potential (CC_0), the first-order TSE (CC_1), and the second-order TSE (CC_2), were computed. For comparison, the correlation coefficient (CC_{SL}) between the surface Laplacian method of (3) and the exact cortical surface potential was also computed. We show CC_0 explicitly as

$$CC_0 = \frac{\sum(\Phi_c[n] - \bar{\Phi}_c)(\Phi_x[n] - \bar{\Phi}_x)}{\left(\sum(\Phi_c[n] - \bar{\Phi}_c)^2 \sum(\Phi_x[n] - \bar{\Phi}_x)^2\right)^{1/2}} \tag{45}$$

where $\Phi_c[n]$ and $\Phi_x[n]$ are the potentials at electrode n on the scalp and cortical surface, respectively, the sums run over all electrodes, and $\bar{\Phi}_c$ and $\bar{\Phi}_x$ are the potentials averaged over all scalp and cortical electrodes, respectively. The expressions for the other CCs are similar. The mean CCs, averaged over 100 examples with random background scalp potentials, are listed in Table II.

In Fig. 3(a), we show an example of the scalp surface potential distribution. Qualitatively, the TSE method [Figs. 3(c) and (d)] sharpens the broad scalp surface potential and better approximates the exact cortical surface potential [Fig. 3(b)]. The improvement to the scalp surface potential is made quantitative in the CCs of Table II. For noiseless data, the TSE approximation significantly increases the mean CC of the scalp surface potential. The TSE method also improves the mean CC of the surface Laplacian method (3). The results for the noisy scalp data are also listed in Table II.

The quantitative improvement of the TSE method over the traditional surface Laplacian method in (3) is revealed by the mean Euclidian error (EE) values in Table III. By Euclidian error, we mean

$$EE = \frac{||\Phi_i - \Phi_x||}{||\Phi_x||} \tag{46}$$

TABLE III
MEAN EUCLIDEAN ERRORS

Noise	$\mathbf{EE}_0(\times 10^3)$	$\mathbf{EE}_1(\times 10^3)$	$\mathbf{EE}_2(\times 10^3)$	$\mathbf{EE}_{\mathrm{SL}}(\times 10^3)$
None	4.5 ± 0.1	3.5 ± 0.1	3.5 ± 0.1	16.2 ± 0.1
10%	4.6 ± 0.2	3.9 ± 0.2	3.9 ± 0.2	13.5 ± 0.2

The mean EEs (46) between the exact cortical surface potential and: the scalp surface potential ($\mathbf{EE}_0$), the first order TSE ($\mathbf{EE}_1$), the second order TSE ($\mathbf{EE}_2$), and the traditional surface Laplacian method ($\mathbf{EE}_{\mathrm{SL}}$). The results are averaged over 100 examples of random background scalp potentials. In the first row, the noiseless scalp potential was deblurred. In the second row, 10% white noise was added to the scalp potential before deblurring.

where Φ_x is the exact cortical surface potential, Φ_i is a potential distribution evaluated at the same electrode configuration, and $||\Phi||$ is

$$||\Phi|| = \sum_{n=1}^{N_e} \sqrt{\Phi[n]^2} \tag{47}$$

where N_e is the total number of electrodes and $\Phi[n]$ is the potential at electrode n. As above, we computed the EE between the exact cortical surface potential and: the scalp surface potential (EE_0), the first-order TSE (EE_1), and the second-order TSE (EE_2). For comparison, we also computed the EE between and the surface Laplacian method in (3) and the exact cortical surface potential ($\mathrm{EE}_{\mathrm{SL}}$). The mean EEs, averaged over 100 examples of random background scalp potentials, are listed in Table III. We found that, for noiseless scalp data, the TSE method reduced the mean EE of the scalp surface potential. Moreover, the TSE method reduced the mean EE of the surface Laplacian method by nearly a factor of 5. Similar results, listed in Table III, hold for the noisy scalp data.

At this point the reader may wonder why $\mathrm{EE}_{\mathrm{SL}}$ is so large. The reason for this is that the surface Laplacian operator amplifies higher order spherical harmonics in the scalp surface potential by a factor that is too big. Thus, the difference in magnitude between the surface Laplacian approximation and the exact cortical surface potential is large. This difference in magnitude does not effect $\mathrm{CC}_{\mathrm{SL}}$, but is clearly revealed in $\mathrm{EE}_{\mathrm{SL}}$. For this reason, $\mathrm{EE}_{\mathrm{SL}}$ is greater than EE_0, although the surface Laplacian approximation does correlate well with the exact cortical surface potential. The TSE method improves both the CC and the EE of the scalp surface potential. Thus, we claim that the TSE result is quantitative while the surface Laplacian method in (3) is only proportional. Quantitative knowledge of the cortical surface potential may be useful when making comparisons across subjects. For example, the power spectrum (with units μV) is known to be different in different subjects, but it is usually unclear whether this is due to differences in neurophysiology or merely differences in head volume conduction properties [12]. The TSE method could allow direct neurophysiological comparisons, provided an accurate head model is known. Thus, in comparisons across clinical subjects, it may be useful to develop a quantitative cortical surface potential estimate.

The TSE algorithm provides a better quantitative approximation to the cortical surface potential than the scalp surface potential or the surface Laplacian in (3). In the simulations above, inclusion of the biharmonic correction in (23)—the $\nabla_{||}^4$ term—does not significantly improve the approximation of the TSE method. The importance of the biharmonic correction becomes significant when high spatial frequencies ($L > 17$) are detectable on the scalp, as discussed in Appendix I.

V. DISCUSSION

The analysis in Section IV shows that the TSE method provides a more accurate estimation of the cortical surface potential than the surface Laplacian in (3). The improvement is most clearly displayed in the EE values of Table III; the TSE method reduces the EE by approximately a factor of five compared to the surface Laplacian method. The reduced Euclidian errors are due to the quantitative formulation of the TSE method. Unlike (3), the TSE method is model-dependent, but the conductivities and interface radii may be specified locally for each electrode. The local nature of the TSE method produces a four-shell spherical head model with conductivities and radii appropriate to each electrode. The TSE method is flexible and allows for realistic variations in the conductivities and radii, which can be experimentally determined through electrical impedance tomography [7].

There are shortcomings to the TSE method and SL methods in general. In Section III, we applied the TSE method to the simple four-shell spherical head model. We show in Appendix II how the TSE method can be extended to more realistic geometries. A drawback of the TSE and other SL methods is that analytic expressions for the SL become more cumbersome as the geometry becomes more realistic. Also, noise often gives rise to the highest spatial frequencies in experimental scalp surface potential data. This noise will be amplified by the SL, and even more so by the surface biharmonic, in (23). As mentioned in Section IV-D, we can account for noisy scalp surface potential data by a regularization (or smoothing) of the spline interpolation. This regularization is a cumbersome and computationally expensive procedure. Finally, unlike boundary element methods, the TSE method ignores boundary conditions introduced by the recording electrodes. Even with these drawbacks the TSE method offers a straight forward and rigorous means of deblurring the scalp surface potential.

APPENDIX I
IMPORTANCE OF $\nabla_{||}^4$

In this Appendix, we will show that the $\nabla_{||}^4$ term in (23) becomes important when there are components of the signal with $L \geq 17$. From (23), we have

$$\Phi_x \approx \Phi_0 - 0.095\nabla_{||}^2\Phi_0 + 3.1 \times 10^{-5}\nabla_{||}^4\Phi_0. \tag{48}$$

The $\nabla_{||}^4$ term in (48) becomes significant in the approximation when the third term is 10% of the second term, i.e., when

$$||\nabla_{||}^4\Phi_0|| \approx 308||\nabla_{||}^2\Phi_0||. \tag{49}$$

The scalp surface potential Φ_0 can be expressed in terms of Legendre polynomials, as in (28) or (41). The application of $\nabla_{||}^2$ or $\nabla_{||}^4$ to a Legendre polynomial of order L introduces a factor of $-L(L+1)$ or $L^2(L+1)^2$, respectively. Hence (49) becomes

$$(L(L+1))^2 \approx 308(L(L+1)). \tag{50}$$

This expression is satisfied when $L = 17$. Thus, the biharmonic term becomes an important correction to the surface Laplacian in the TSE method when we can detect Legendre polynomials of order 17 and greater. This analysis is easily extended to cortical measurements (36).

APPENDIX II
EXTENSION TO MORE REALISTIC GEOMETRIES

In Section III, we applied the TSE method to the simple four-shell spherical head model. We show in this Appendix how the TSE method applies to more general geometries. Consider the interface between two regions with uniform conductivities σ_1 and σ_2, respectively. We can define a local orthogonal curvilinear coordinate system with one axis $\xi_\perp$ perpendicular to the interface and two axes $\xi_\parallel$ parallel to the interface. Knowing the potential $\Phi_1[\xi_\parallel, \xi_\perp]$ in region 1, we write a TSE in $\xi_\perp$ for the unknown potential $\Phi_2[\xi_\parallel, \xi_\perp]$ in region 2 as

$$\Phi_2[\xi_\parallel, \xi_\perp] = \Phi_2[\xi_\parallel, \xi_\perp^0] + (\xi_\perp - \xi_\perp^0)\partial_{\xi_\perp}\Phi_2[\xi_\parallel, \xi_\perp]\big|_{\xi_\perp^0} + \frac{1}{2}(\xi_\perp - \xi_\perp^0)^2\partial_{\xi_\perp}^2\Phi_2[\xi_\parallel, \xi_\perp]\big|_{\xi_\perp^0} + O[(\xi_\perp - \xi_\perp^0)^3] \quad (51)$$

where $\xi_\perp^0$ is the location of the interface along $\xi_\perp$. The boundary conditions are equivalent to those in (6) and (7) and are given as follows:

$$\Phi_2[\xi_\parallel, \xi_\perp^0] = \Phi_1[\xi_\parallel, \xi_\perp^0]$$
$$\partial_{\xi_\perp}\Phi_2[\xi_\parallel, \xi_\perp]\big|_{\xi_\perp^0} = \frac{\sigma_1}{\sigma_2}\partial_{\xi_\perp}\Phi_1[\xi_\parallel, \xi_\perp]\big|_{\xi_\perp^0}. \quad (52)$$

Here, we obtain expressions for the first two terms of (51) using the known quantity $\Phi_1[\xi_\parallel, \xi_\perp]$. An expression for the third term in (51) may be derived from Laplace's equation

$$\left(\partial_{\xi_\perp}\left(\frac{h_2 h_3}{h_1}\partial_{\xi_\perp}\right) + \nabla_\parallel^2\right)\Phi_2 = 0. \quad (53)$$

Here, we have written the Laplacian in general form for orthogonal curvilinear coordinates and grouped all derivatives tangential to the interface in $\nabla_\parallel^2$. The terms h_1, h_2, and h_3 are the usual scale factors. We expand and rearrange (53) to obtain

$$\partial_{\xi_\perp}^2 = -\frac{1}{H}\frac{\partial H}{\partial \xi_\perp}\partial_{\xi_\perp} - \frac{1}{H}\nabla_\parallel^2 \quad (54)$$

where $H = h_2 h_3 / h_1$. Then (51) can be written as

$$\Phi_2[\xi_\parallel, \xi_\perp] = \Phi_1[\xi_\parallel, \xi_\perp^0] + (\xi_\perp - \xi_\perp^0)\frac{\sigma_1}{\sigma_2}\partial_{\xi_\perp}\Phi_1[\xi_\parallel, \xi_\perp]\big|_{\xi_\perp^0} - \frac{1}{2}(\xi_\perp - \xi_\perp^0)^2\left(\frac{1}{H}\frac{\partial H}{\partial \xi_\perp}\frac{\sigma_1}{\sigma_2}\partial_{\xi_\perp}\Phi_1[\xi_\parallel, \xi_\perp]\big|_{\xi_\perp^0} + \frac{1}{H}\nabla_\parallel^2\Phi_1[\xi_\parallel, \xi_\perp]\big|_{\xi_\perp^0}\right) + O[(\xi_\perp - \xi_\perp^0)^3] \quad (55)$$

where we have made use of the boundary conditions. In (55), we have expressed the unknown quantity $\Phi_2[\xi_\parallel, \xi_\perp]$ in terms of the known quantity $\Phi_1[\xi_\parallel, \xi_\perp]$. The TSE method may be extended to nonspherical geometries by replacing (4) with (55) and proceeding as in Section III.

ACKNOWLEDGMENT

The authors would like to thank E. Edwards, R. Knight, and T. Ferree for many useful discussions, P. Nunez for helpful references, and D. Hudson and M. Cohen for their encouragement.

REFERENCES

[1] R. B. Kearfott, R. D. Sidman, D. A. Major, and C. D. Hill, "Numerical tests of a method for simulating electric potentials on the cortical surface," *IEEE Trans. Biomed. Eng.*, vol. 38, pp. 294–299, Mar. 1991.
[2] G. Edlinger, P. Wach, and G. Pfurtscheller, "On the realization of an analytic high-resolution EEG," *IEEE Trans. Biomed. Eng.*, vol. 45, pp. 736–745, June 1998.
[3] S. K. Law, P. Nunez, and R. Wijesinghe, "High-resolution EEG using spline generated surface laplacians on spherical and ellipsoidal surfaces," *IEEE Trans. Biomed. Eng.*, vol. 40, pp. 145–153, Feb. 1993.
[4] P. L. Nunez, R. Silberstein, P. Cadusch, R. Wijesinghe, A. Westdorp, and R. Srinivasan, "A theoretical and experimatnal study of high resolution EEG based on surface laplacians and cortical imaging," *Electroenceph. Clin. Neurophysiol.*, vol. 90, pp. 40–57, Aug. 1994.
[5] B. Hjorth, "An on line transformation of EEG scalp potentials into orthogonal source derivations," *Electroenceph. Clin. Neurophysiol.*, vol. 39, pp. 526–530, July 1975.
[6] F. Babiloni, F. Cincotti, F. Carducci, P. M. Rossini, and C. Babiloni, "Spatial enhancement of EEG data by surface laplacian estimation: The use of magnetic resonance imaging based head models," *Electroenceph. Clin. Neurophysiol.*, vol. 112, pp. 724–727, May 2001.
[7] M. T. Clay and T. C. Ferree, "Weighted regularization in electrical impedance tomography with applications to acute cerebral stroke," *IEEE Trans. Biomed. Eng.*, vol. 21, pp. 629–637, June 2002.
[8] J. D. Jackson, *Classical Electrodynamics*. New York: Wiley, 1999.
[9] P. L. Nunez, *Electric Fields of the Brain: The Neurophysics of EEG*. New York: Oxford Univ. Press, 1981.
[10] R. D. Pascual-Marqui, S. L. Gonzalez-Andino, P. Valdes-Sosa, and R. Biscay-Lirio, "Current source density estimation and interpolation based on the spherical harmonic fourier expansion," *Int. J. Neurosci.*, vol. 43, pp. 237–249, Dec. 1988.
[11] G. Wahba, "Spline interpolation and smoothing on the sphere," *SIAM J. Sci. Stat. Comput.*, vol. 2, pp. 5–16, Mar. 1981.
[12] T. Ferree, private communication, 2003.

Mark A. Kramer received the B.A. degree in physics from Oberlin College, Oberlin, OH, in 2001. He is currently working towards the Ph.D. degree in applied physics in the Applied Science and Technology Graduate Group at the University of California, Berkeley.

Andrew J. Szeri received the Ph.D. degree in theoretical and applied mechanics from Cornell University, Ithaca, NY, in 1988.

He is a Professor of Mechanical Engineering and member of the Graduate Group in Applied Science and Technology, University of California, Berkeley. His research interests include nonlinear dynamics and fluid mechanics, with applications in biomedical engineering and cavitation physics.